Fermi National Accelerator Laboratory

FERMILAB-Conf-95/241-E
CDF

Wγ and Zγ Production at the Tevatron

Doug Benjamin
For the CDF Collaboration

Fermi National Accelerator Laboratory
P.O. Box 500, Batavia, Illinois 60510

Texas Tech University
P.O. Box 41051, Lubbock, Texas 79409

July 1995

Published Proceedings of the *10th Topical Workshop on Proton-Antiproton Collider Physics*, Fermilab, Batavia, Illinois, May 9-13, 1995

Disclaimer

CDF/ANAL/ELECTROWEAK/PUB/3191

FERMILAB-CONF-95/241-E

$W\gamma$ and $Z\gamma$ production at the Tevatron

Doug Benjamin
Texas Tech University
P.O. Box 41051
Lubbock, Tx 79409

Abstract

$W\gamma$ and $Z\gamma$ production in $\bar{p}p$ collisions at $\sqrt{s} = 1.8$ TeV have been studied by the CDF and DØ collaborations. Direct measurements of the $WW\gamma$ couplings and limits on the $ZZ\gamma$ couplings based on the study of $\bar{p}p \to \ell\nu\gamma + X$ and $\bar{p}p \to \ell\ell\gamma + X$ events, respectively, from the 1992-1993 and first part of the 1994 runs of the Fermilab Tevatron Collider are presented here.

Introduction

The measurement of the self-interactions of the electro-weak gauge bosons (γ, W and Z) provides a crucial test of the Standard Model. *Direct* measurements of this self-interaction are possible by studying diboson production such as $W\gamma$ and $Z\gamma$.

The $W\gamma$ process can be described by a general effective lagrangian [1] [2] invariant under $SU(2) \times U(1)$ symmetry. This lagrangian contains four coupling parameters, two *CP-conserving* κ_f and λ_f and two *CP-violating* $\tilde{\kappa}_f$ and $\tilde{\lambda}_f$.

$$\begin{aligned}\mathcal{L}_{WW\gamma} &= -ie\Bigg[\left(W^{\dagger}_{\mu\nu}W^{\mu}A^{\nu} - W^{\dagger}_{\mu}A_{\nu}W^{\mu\nu}\right) + \kappa_f W^{\dagger}_{\mu}W_{\nu}F^{\mu\nu} \\ &\quad + \frac{\lambda_f}{M_W^2}W^{\dagger}_{\lambda\mu}W^{\mu}_{\nu}F^{\nu\lambda} + \tilde{\kappa}_f W^{\dagger}_{\mu}W_{\nu}\tilde{F}^{\mu\nu} + \frac{\tilde{\lambda}_f}{M_W^2}W^{\dagger}_{\lambda\mu}W^{\mu}_{\nu}\tilde{F}^{\nu\lambda}\Bigg]\end{aligned}$$

where $A^{\mu} = (A^{\mu\dagger})$ and W^{μ} are the photon and W^{-} fields, respectively, and $W_{\mu\nu} = \partial_{\mu}W_{\nu} - \partial_{\nu}W_{\mu}$, $F_{\mu\nu} = \partial_{\mu}A_{\nu} - \partial_{\nu}A_{\mu}$, $\tilde{F}_{\mu\nu} = \frac{1}{2}\epsilon_{\mu\nu\rho\sigma}F^{\rho\sigma}$, e is the charge of the proton, and M_W is the W mass. The terms κ_f,λ_f,$\tilde{\kappa}_f$ and $\tilde{\lambda}_f$, are momentum dependent form factors between the photon and W fields. They are assumed to be of the form:

$$a_f(P^2 = \hat{s},\, \bar{q}^2 = M_W^2,\, q^2 = 0) = \frac{a_{\circ}}{(1 + \frac{\hat{s}}{\Lambda_W^2})^n},$$

where $a_{\circ}$ is the anomalous parameters $\Delta\kappa \equiv \kappa - 1$, λ, $\tilde{\kappa}$ and $\tilde{\lambda}$, $\hat{s}$ is the square of the invariant mass of the photon and W, Λ_W is the W form factor scale and $n = 2$ for the dipole for factor. [2] The choice of $n = 2$ guarantees unitarity at high energies and implies that the couplings vanish as $\hat{s}$ becomes large. The tree level Standard Model predicts $\Delta\kappa = \lambda = \tilde{\kappa} = \tilde{\lambda} = 0$.

The $Z\gamma$ interaction can be described by the general $ZZ\gamma$ vertex function containing a set of four couplings, two *CP-conserving* h_3^Z and h_4^Z and two *CP-violating* h_1^Z and h_2^Z.

$$\begin{aligned}\Gamma^{\alpha\beta\mu}_{ZZ\gamma}(q_1, q_2, P) &= \left(\frac{P^2 - q_1^2}{M_Z^2}\right) \times [h_1^Z(q_2^{\mu}g^{\alpha\beta} - q_2^{\alpha}g^{\mu\beta}) + \frac{h_2^Z}{M_Z^2}P^{\alpha} \\ &\quad (P \cdot q_2 g^{\mu\beta} - q_2^{\mu}P^{\beta}) + h_3^Z\epsilon^{\mu\alpha\beta\rho}q_{2\rho} + \frac{h_4^Z}{M_Z^2}P^{\alpha}\epsilon^{\mu\alpha\beta\sigma}P_{\rho}q_{2\sigma}]\end{aligned}$$

[1] where M_Z is the Z mass, P and q_1 are the incoming and outgoing Z four-momenta and q_2 is the four-momenta of the outgoing photon. The variables h_i^Z,where $i = 1-4$, are the momentum dependent form factors. Like the the $W\gamma$ case, they are assumed to be of the form:

$$a_f(P^2 = \hat{s},\, q_1^2 = M_Z^2,\, q_2^2 = 0) = \frac{h_{i0}^Z}{(1 + \frac{\hat{s}}{\Lambda_Z^2})^n},$$

where Λ_Z^2 is the Z form factor scale and is expected to be on the order of at least a few hundred GeV. In order to preserve unitarity are high energies: $n = 3$ for $h_{1,3}^Z$ and $n = 4$ for $h_{2,4}^Z$. [3] The values h_{i0}^Z represent the low energy limits $\hat{s} = 0$ of the $Z\gamma$ couplings. The Standard Model predicts: $h_{10}^Z = h_{20}^Z = h_{30}^Z = h_{40}^Z = 0$. (ie. the Z should not couple to the photon).

The studies of the $W\gamma$ and $Z\gamma$ couplings are based on $\bar{p}p \rightarrow \ell\nu\gamma + X$ and $\bar{p}p \rightarrow \ell\ell\gamma + X$ ($\ell = e, \nu$) events observed in the CDF and DØ detectors. Anomalous coupling parameters enhance the both $W\gamma$ and $Z\gamma$ production at large $\hat{s}$ and thereby result in an excess of events with high transverse energy photons (E_T^γ) well separated from the charged leptons.

Photon Detection at CDF and DØ

The detection of photons are crucial to the study of $W\gamma$ and $Z\gamma$ production. Both collaborations identify photons as isolated clusters of energy in their respective calorimeters with: *(i)* large electromagnetic fraction; *(ii)* shower shapes consistent with single photons and *(iii)* no tracks pointing at the cluster. Table 1 summarizes the photon detection for both groups.

Both CDF and DØ find that the photon detection efficiency is a function of E_T^γ. The overall photon detection efficiency includes terms for photon efficiency; the probability of not detecting the photon due to its conversion into a e^+e^- pair; the probability that the photon will be rejected due to overlap with a random track in the event and the probability that the photon will be rejected due to random energy from the underlying event. This can be written as $\epsilon^\gamma = \epsilon_{cal}(E_T^\gamma) \times (1 - Prob(\gamma \rightarrow ee)) \times (1 - Prob(\text{track overlap})) \times (1 - Prob(\text{energy overlap}))$ The overall photon detection efficiency is summarized in table 2.

Table 1: Photon detection at CDF and DØ

	CDF	**DØ**
detection	$\|\eta\| < 1.0$	$\|\eta\| < 1.1$
region		$1.5 < \|\eta\| < 2.5$
$E_T^\gamma >$	7 GeV	10 GeV
EM fraction	$HAD/EM < 0.055 + 0.00045 \times E(\text{GeV})$	$EM/Total > 0.9$
Isolation	$\frac{E_T(0.4)-E_T^\gamma}{E_T^\gamma} < 0.15$	$\frac{E(0.4)-EM(0.2)}{EM(0.2)} < 0.1$
	$\sum P_T^{tracks}(0.4) < 2\,\text{GeV}/c$	
Shower Shape	transverse	longitudinal/transverse
	No matching tracks	No matching tracks

Table 2: Overall Photon Detection Efficiency

	CDF	**DØ**	
E_T^γ	$\|\eta\| < 1.1$	$\|\eta\| < 1.1$	$1.5 < \|\eta\| < 2.5$
$> 25GeV$	0.804 ± 0.023	0.74 ± 0.05	0.58 ± 0.05
$= 10$		0.43 ± 0.04	0.38 ± 0.03
$= 7$	0.731 ± 0.021		

$W\gamma$ Couplings

The $W\gamma$ candidate events were selected by requiring: an isolated high p_T lepton; large $\not\!\!E_T$ and an isolated photon. Table 3 summarizes the kinematic and geometric properties of the $W\gamma$ event selection.

Table 3: $W\gamma$ Event Selection

	CDF $\sim 67\ pb^{-1}$		DØ $\sim 14\ pb^{-1}$	
	$e\nu\gamma$	$\mu\nu\gamma$	$e\nu\gamma$	$\mu\nu\gamma$
Geometry	$\lvert\eta_e\rvert < 1.1$	$\lvert\eta_\mu\rvert < 0.6$	$\lvert\eta_e\rvert < 1.1$	$\lvert\eta_\mu\rvert < 1.7$
			$1.5 < \lvert\eta_e\rvert < 2.5$	
Kinematics	$E_T^e > 20$	$p_T^\mu > 20$	$E_T^e > 25$	$p_T^\mu > 15$
(in GeV)	$\not\!\!E_T > 20$	$\not\!\!E_T > 20$	$\not\!\!E_T > 25$	$\not\!\!E_T > 15$
	$E_T^\gamma > 7$ GeV		$E_T^\gamma > 10$ GeV	
	$\Delta R_{\ell\gamma} > 0.7$		$\Delta R_{\ell\gamma} > 0.7$	
	$\Delta R_{\ell\gamma} = \sqrt{(\Delta\eta_{\ell\gamma})^2 + (\Delta\phi_{\ell\gamma})^2}$			
	$\lvert\eta^\gamma\rvert < 1.1$		$\lvert\eta^\gamma\rvert < 1.1$, $1.5 < \lvert\eta_\gamma\rvert < 2.5$	

The backgrounds to $W\gamma$ production include: W + jet events where a jet mimics an isolated photon; $Z\gamma$ events where one of the decay leptons of the Z is not found or is mis-measured and contributes to a large value of $\not\!\!E_T$ and $W\gamma$ events where $W \to \tau\nu$ and $\tau \to \ell\nu\bar{\nu}$. The largest background (W + jets) is estimated from the W + jets data using a fragmentation probability $\mathcal{P}(jet \to \text{“}\gamma\text{”})$. This function (measured from independent data samples) is probability that a jet will pass all photon selection cuts including isolation and is a function of E_T^{jet}. The other two backgrounds are estimated from Monte Carlo.

A $W\gamma$ Monte Carlo [4] was used to generate simulated events. This Monte Carlo program includes both $W\gamma$ production and radiative decay including interference effects; the events are generated to leading order and higher order QCD effects are approximated a K-factor. Both CDF and DØ used the MRSD-' structure functions and simulated the p_T of the $W\gamma$ system using the spectrum from the inclusive W samples. The generated events underwent detector simulation. Table 4 summarizes $W\gamma$ production for both collaborations. One can see that both groups find good agreement with the standard model for each channel and for the combined results.

Table 4: Summary $W\gamma$ production

	CDF preliminary $\sim 67\,pb^{-1}$		DØ preliminary $\sim 14\,pb^{-1}$	
	$e\nu\gamma$	$\mu\nu\gamma$	$e\nu\gamma$	$\mu\nu\gamma$
$N_{\rm DATA}$	75	34	11	12
Bkgd	16.1 ± 2.4	10.3 ± 1.2	2.0 ± 0.9	4.4 ± 1.1
Signal	$58.9 \pm 9.0 \pm 2.6$	$23.7 \pm 5.9 \pm 1.1$	$9.0^{+4.2}_{-3.1} \pm 0.9$	$7.6^{+4.4}_{-3.2} \pm 1.1$
SM	53.5 ± 6.8	21.8 ± 4.3	8.2 ± 1.3	7.8 ± 1.4
$\sigma \cdot BR$	20.5 ± 3.6	21.5 ± 5.7	$15.7^{+7.8}_{-6.0}$	$13.6^{+8.4}_{-6.5}$
	$(E_T^\gamma > 7\text{GeV})$		$(E_T^\gamma > 10\text{GeV})$	
$e + \mu$	$20.7 \pm 2.9 \pm 0.7$		$14.8^{+5.9}_{-4.6}$	
SM	18.6 ± 2.9		18.4 ± 1.1	
	Both Experiments agree with SM			

Figures 1 and 2 compare the data to the sum of the Standard Model prediction and the estimated background in the distributions of E_T^γ, $\Delta R_{\ell\gamma}$ and the cluster transverse mass. The cluster transverse mass is defined by $M^2_{CT_W} = [(M^2_{\ell\gamma} + |\vec{P}_T^{\,\gamma} + \vec{P}_T^{\,\ell}|^2)^{\frac{1}{2}} + \vec{P}_T^{\,\nu_\ell}]^2 - |\vec{P}_T^{\,\gamma} + \vec{P}_T^{\,\ell} + \vec{P}_T^{\,\nu_\ell}|^2$ The absence of an excess of high E_T photons precludes large deviations from the Standard Model couplings.

Limits on $WW\gamma$ anomalous couplings were evaluated by comparing the observed photon E_T distribution to the sum of the Monte Carlo signal prediction plus the estimated background. The likelihood that this sum could fluctuate to the observed number of events was calculated for each E_T bin using Poisson statistics. The predicted number of events was convoluted with a Gaussian distribution to include the effects of systematic uncertainties. The 95% confidence contours in $\Delta\kappa$ and λ are shown in figure 3. Assuming that only one coupling is non-zero at at a time the current limits (@95% CL) of the CP-conserving anomalous $WW\gamma$ couplings are summarized in table 5.

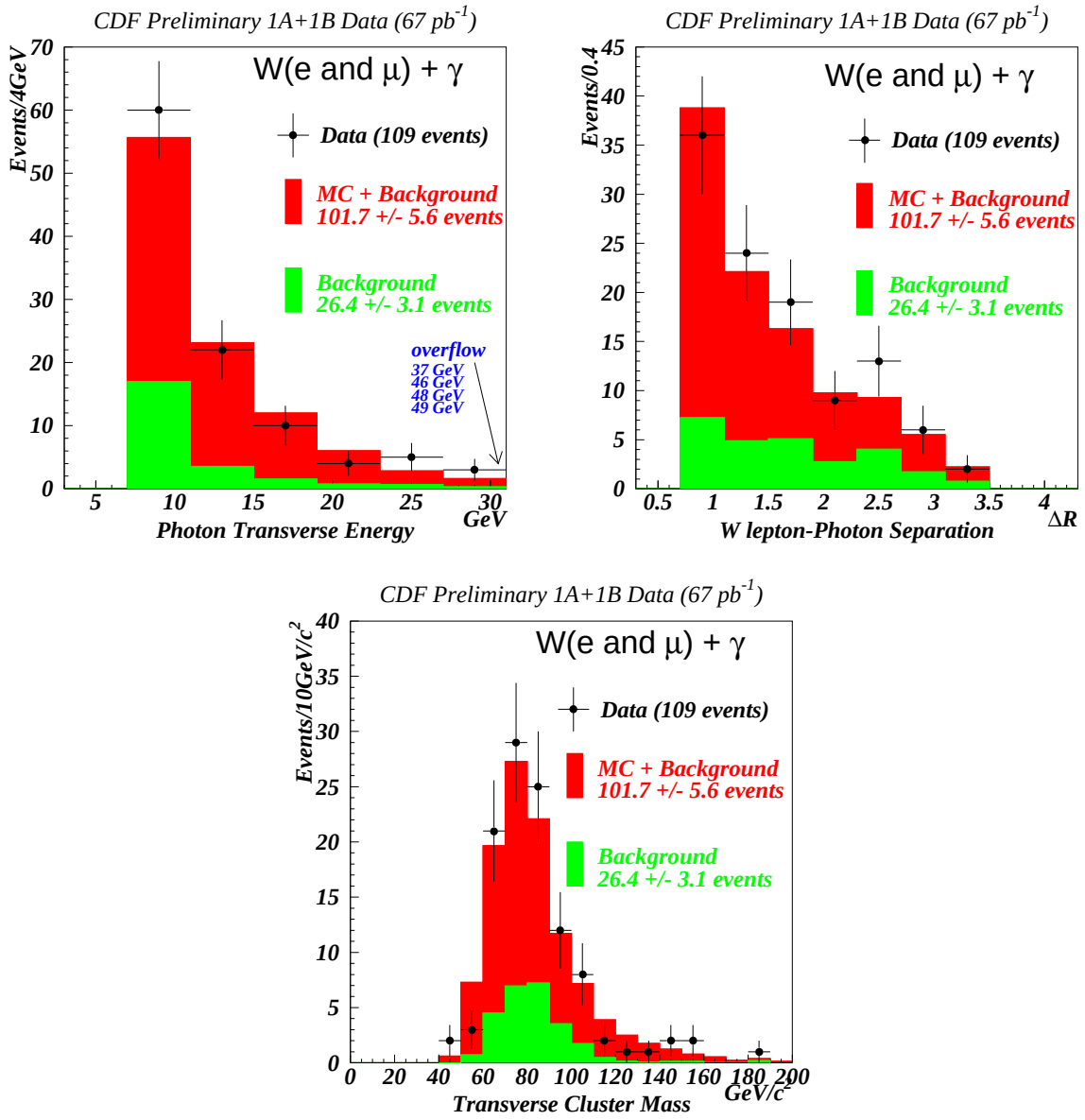

Figure 1: CDF distribution of (a) E_T^γ, (b) $\Delta R_{\ell\gamma}$ and (c) M_{CT_W} for the combined electron and muon data sample. The points are the data. The dark grey histograms represent the expected Standard Model signal plus the estimated background. The light grey histogram represents the background estimate.

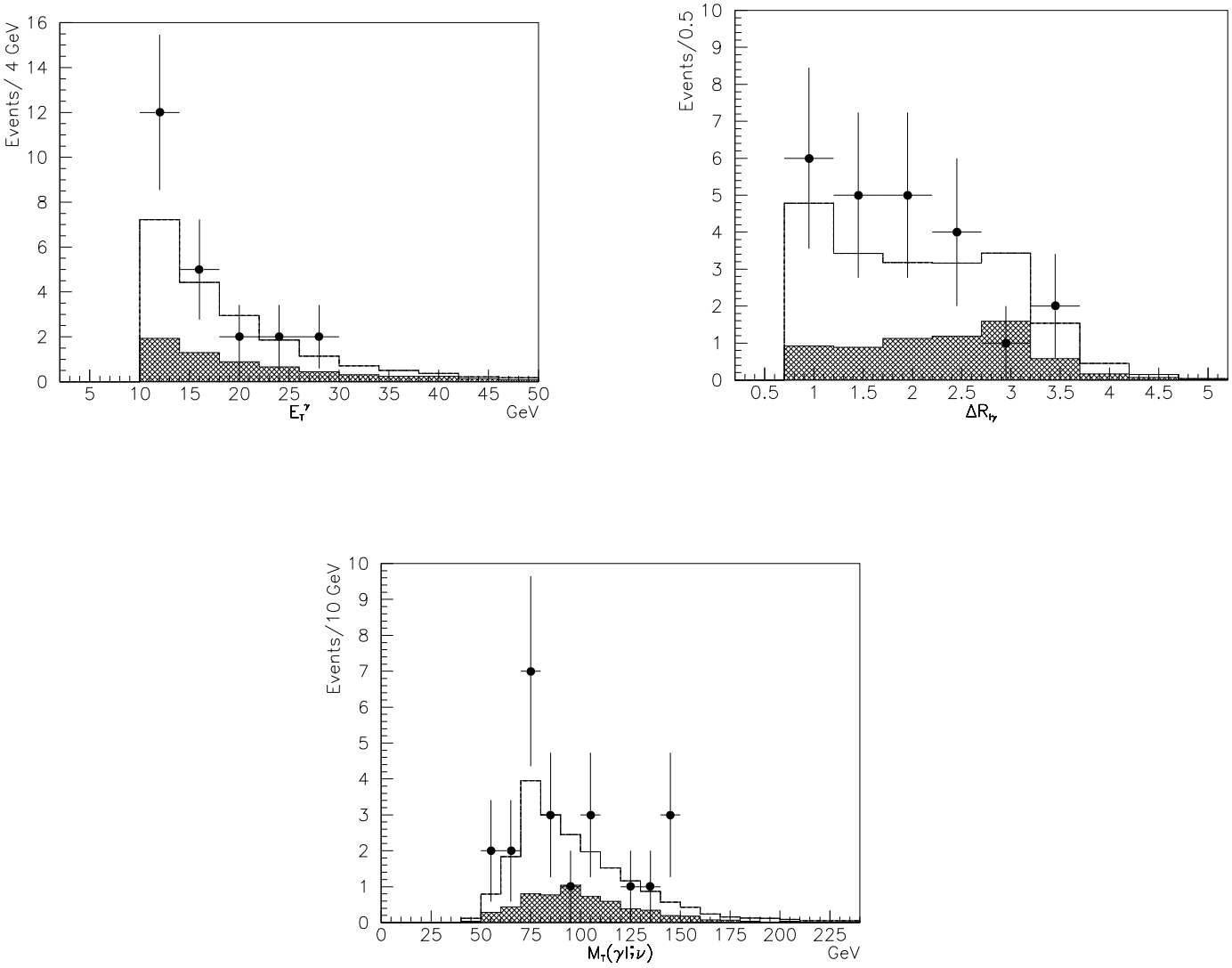

Figure 2: DØ distribution of (a) E_T^γ, (b) $\Delta R_{\ell\gamma}$ and (c) M_{CT_W} for the combined electron and muon data sample. The points are the data. The open histograms represents the expected Standard Model signal plus the estimated background. The shaded histograms represents the background estimate.

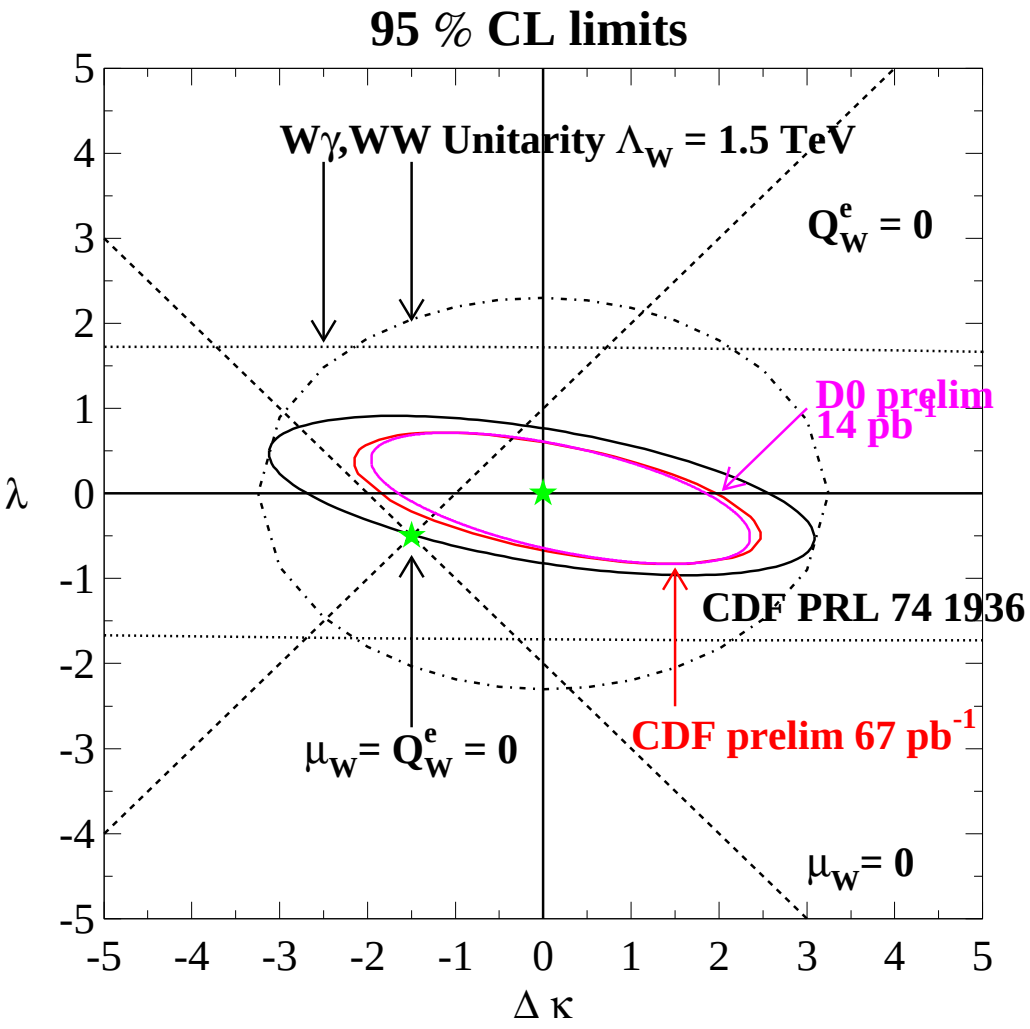

Figure 3: Limits on CP-conserving anomalous $WW\gamma$ couplings. The ellipses represent the 95% exclusion contours. The W^+W^- and $W\gamma$ unitarity limits for a form factor scale $\Lambda_W = 1.5$TeV are indicated by dotted-dashed and dotted curves, respectively. The current limits from CDF and DØ are shown together with the previous limit from CDF

Table 5: (95% CL) of the CP-conserving anomalous $WW\gamma$ couplings

	$(\lambda = 0)$	$(\Delta\kappa = 0)$
DØ *p*relim.	$-1.6 < \Delta\kappa < 1.8$	$-0.6 < \lambda < 0.6$
CDF *p*relim.	$-1.8 < \Delta\kappa < 2.0$	$-0.7 < \lambda < 0.6$

$Z\gamma$ Couplings

The $Z\gamma$ candidate events were selected by requiring: two isolated high p_T leptons; and an isolated photon. Table 6 summarizes the kinematic and geometric properties of the $Z\gamma$ event selection. The backgrounds to $Z\gamma$ production include: Z + jet events where a jet mimics an isolated photon and $Z\gamma$ events where $Z \to \tau\tau$ and $\tau \to \ell\nu\bar{\nu}$. The largest background (Z + jets) is estimated from the Z + jets data using a fragmentation probability $\mathcal{P}(jet \to \text{“}\gamma\text{”})$. The other backgrounds are estimated from Monte Carlo.

The Baur and Berger $Z\gamma$ Monte Carlo [3] was used to generate simulated events. The generated events underwent detector simulation. Table 7 summarizes $Z\gamma$ production for both collaborations. One can see that both groups find good agreement with the Standard Model for each channel.

Figures 4 and 5 compare the data to the sum of the Standard Model prediction and the estimated background in the distributions of E_T^γ and $\ell^+\ell^-\gamma$ invariant mass for CDF, and E_T^γ for DØ , respectively.

Limits on $ZZ\gamma$ anomalous couplings were evaluated by comparing the observed photon E_T distribution to the sum of the Monte Carlo signal prediction plus the estimated background. The 95% confidence contours in h_{30}^Z (h_{10}^Z) and h_{40}^Z (h_{20}^Z) are shown in figure 6. Assuming that only one coupling is non-zero at at a time the current limits (@95% CL) of the CP-conserving (CP-violating) anomalous $ZZ\gamma$ couplings are list in table 8.

$W\gamma$ Gauge Zero

Three types of processes give rise to the photon production in W events: radiation from an initial-state quark (u-channel and t-channel), from the W itself (s-channel) and from the charged lepton of the W decay (radiative decay). At large photon scattering angles, θ^*, the u- and t- channel processes

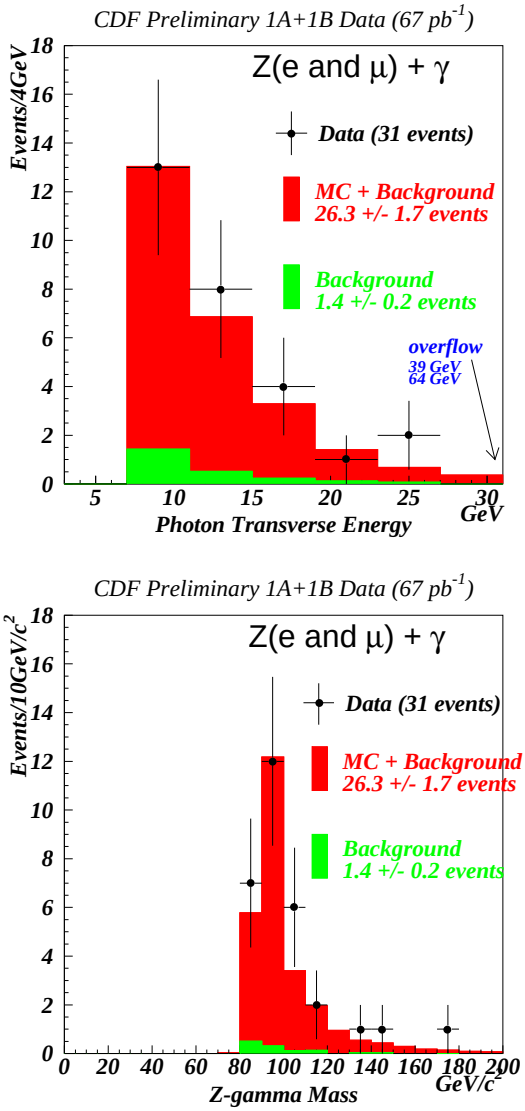

Figure 4: CDF distribution of (a) E_T^γ, (b) $\ell^+\ell^-\gamma$ invariant mass distribution for the electron and muon channels combined. The points are the data. The dark grey histograms represent the expected Standard Model signal plus the estimated background. The light grey histograms represent the background estimate.

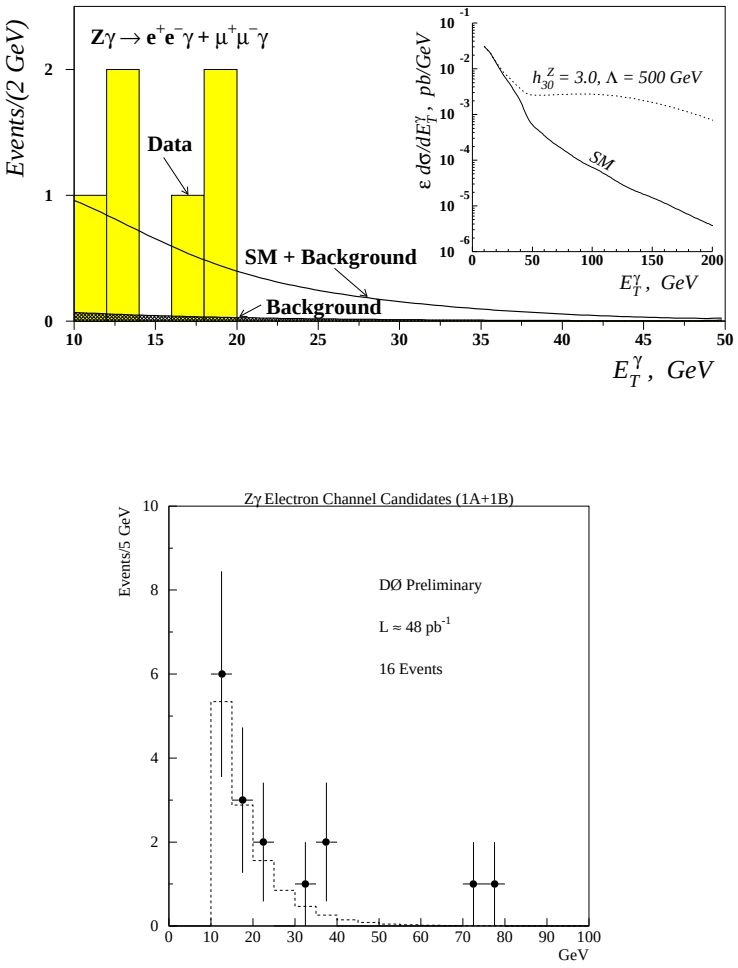

Figure 5: DØ distribution of (a) E_T^γ for the electron and muon channels combined (Fermilab-Pub-95/042-E submitted to PRL). The histogram corresponds to the data, the shaded area represents the estimated background, and the solid line shows the sum of the Standard Model prediction and the background. The insert shows $d\sigma/dE_T^\gamma$ folded with efficiencies from the Standard Model and anomalous ($h_{30}^Z = 3.0$) couplings. (b) E_T^γ for the electron channel from the 92-93 Tevatron run and the first part of the current run. The points are the data and the dashed histogram is the sum of the Standard Model prediction and the background estimate.

Table 6: $Z\gamma$ Event Selection

CDF $\sim 67\,pb^{-1}$		**DØ** $\sim 14\,pb^{-1}$	
$e\nu\gamma$	$\mu\nu\gamma$	$e\nu\gamma$	$\mu\nu\gamma$
$\lvert\eta_{e_1}\rvert < 1.1$	$\lvert\eta_{\mu_1}\rvert < 0.6$	$\lvert\eta_{e_{1,2}}\rvert < 1.1$	$\lvert\eta_{\mu_{1,2}}\rvert < 1.0$
$\lvert\eta_{e_2}\rvert < 4.2$	$\lvert\eta_{\mu_2}\rvert < 1.2$	$1.5 < \lvert\eta_{e_{1,2}}\rvert < 2.5$	
$E_T^{e1} > 20$	$p_T^{\mu 1,2} > 20$	$E_T^{e1,2} > 25$	$p_T^{\mu 1} > 15$
$E_T^{e2} > 20, 15, 10$			$p_T^{\mu 2} > 8$
$E_T^\gamma > 7$ GeV		$E_T^\gamma > 10$ GeV	
$\Delta R_{\ell\gamma} > 0.7$		$\Delta R_{\ell\gamma} > 0.7$	
$\lvert\eta^\gamma\rvert < 1.1$		$\lvert\eta^\gamma\rvert < 1.1$, $1.5 < \lvert\eta_\gamma\rvert < 2.5$	

Table 7: Summary $Z\gamma$ production

	CDF *preliminary* $\sim 67\,pb^{-1}$		**DØ** Fermilab-Pub-95/042-E *submitted to PRL* $\sim 14\,pb^{-1}$		*prelim.* $\sim 48\,pb^{-1}$
	$ee\gamma$	$\mu\mu\gamma$	$ee\gamma$	$\mu\mu\gamma$	$ee\gamma$
$N_{\rm DATA}$	18	13	4	2	16
Bkgd	0.9 ± 0.3	0.5 ± 0.1	0.43 ± 0.06	0.05 ± 0.01	1.2
Sig	17.1 ± 5.7	12.5 ± 3.6	$3.6^{+3.1}_{-1.9}$	$1.9^{+2.6}_{-1.3}$	$14.8^{+5.1}_{-3.1}$
SM	16.2 ± 1.8	8.7 ± 0.7	2.8 ± 0.4	2.3 ± 0.4	11.5 ± 2.4
$\sigma \cdot BR$	5.0 ± 1.8	7.2 ± 2.1			
	($E_T^\gamma > 7$GeV)				
combined	$5.7 \pm 1.4 \pm 0.1$				
SM	4.8 ± 0.6				

Both Experiments agree with SM

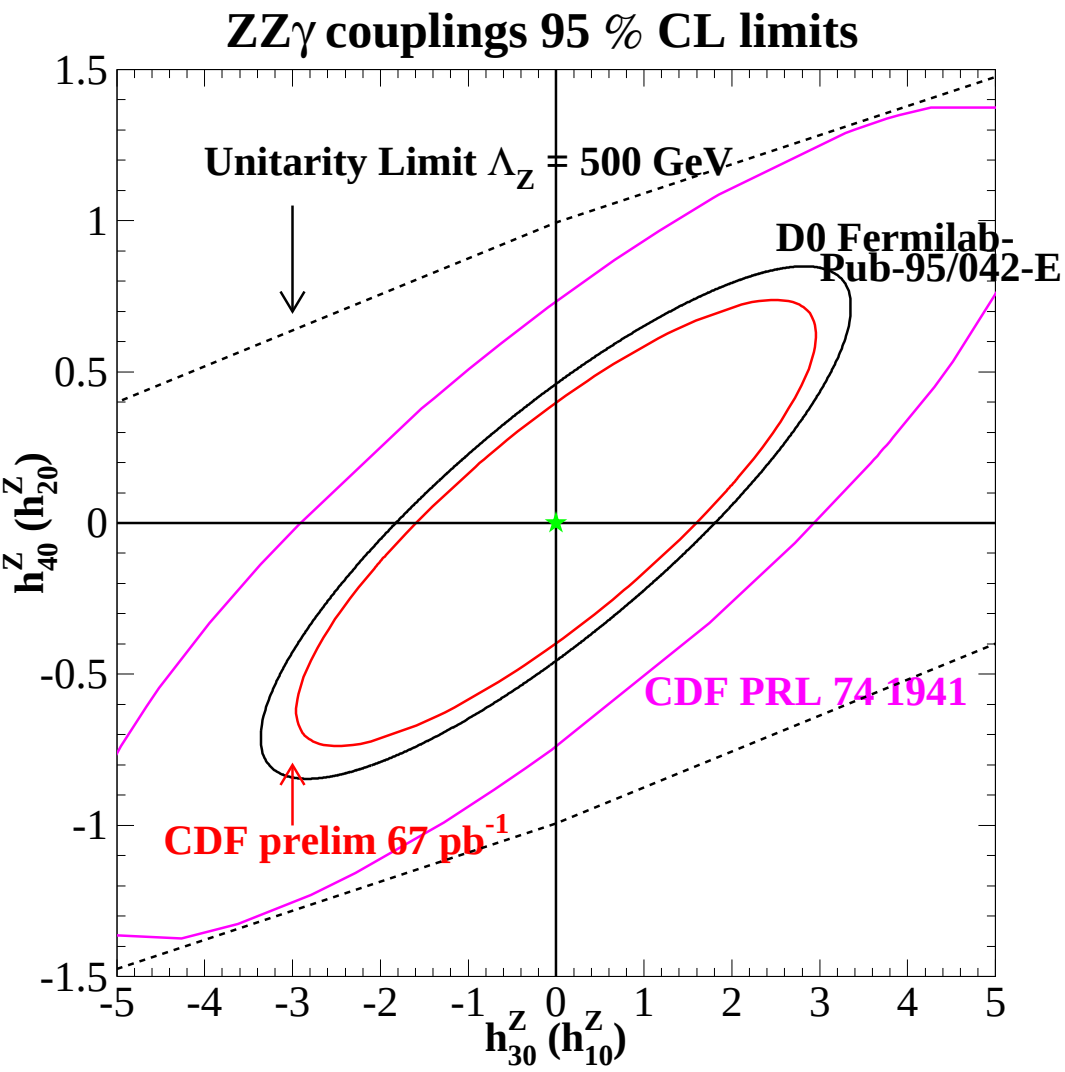

Figure 6: Limits on CP-conserving anomalous $ZZ\gamma$ couplings. The ellipses represent the 95% exclusion contours. The $ZZ\gamma$ unitarity limit for a form factor scale $\Lambda_Z = 500$GeV are indicated by dashed curve, respectively. The current limits from CDF and DØ are shown together with the previous limit from CDF

Table 8: (95% CL) of the anomalous $ZZ\gamma$ couplings

	$[h_{40}^Z\ (h_{20}^Z) = 0]$	$[h_{30}^Z\ (h_{10}^Z) = 0]$
DØ [6]	$-1.9 < h_{30}^Z\ (h_{10}^Z) < 1.8$	$-0.5 < h_{40}^Z\ (h_{20}^Z) < 0.5$
CDF *prelim.*	$-1.6 < h_{30}^Z\ (h_{10}^Z) < 1.6$	$-0.4 < h_{40}^Z\ (h_{20}^Z) < 0.4$

destructively interfere with the s-channel process. θ^* is defined as the angle between the photon and the incoming quark in the $W\gamma$ rest frame. This results in a radiation amplitude zero [5] in the $W^{\mp}\gamma$ differential cross section $d\sigma/d\cos\theta^*$ at $\cos\theta^* = \pm\frac{1}{3}$. The radiative decay process is considered a background to $W\gamma$ production.

In order to determine the $W\gamma$ rest frame, the four-momentum of the ν from $W \to \ell\nu$ must be determined. This is accomplished by mass constraining ($M_{\ell\nu} = M_W$) to determine the ν four-momentum; giving two possible solutions. Since the W is highly polarized at the Tevatron, 73% of the time one can choose correct solution of the ν four-momentum. The p_z^ν is chosen by:

$$P_Z(\nu) = \begin{cases} \min(P_{Z_1}, P_{Z_2}) & \text{for } W^-\gamma \\ \max(P_{Z_1}, P_{Z_2}) & \text{for } W^+\gamma \end{cases}$$

The radiative decay process is suppressed by: 1) making a stringent ΔR cut - $\Delta R > 1.5$ and 2) $M(\ell,\gamma,\nu) \neq M_W$. Table 9 shows the effect of these two cuts on a sample of $W\gamma$ events from CDF. Figure 7 shows the $\cos\theta^*$ distributions of CDF data and Standard Model predictions for the loose ($\Delta R > 0.7$) and tight cuts ($\Delta R > 1.5$ and $M(\ell,\gamma,\nu) \neq M_W$). The $\cos\theta^*$ distributins in figure 7 are charge signed. This means that $\cos\theta^*$ values for W^+ are "flipped" about $\cos\theta^* = 0$; this allows the values of $\cos\theta^*$ for both W^+ and W^- to be plotted on the same horizontal axis.

Conclusion

The CDF and DØ collaborations have studied $W\gamma$ and $Z\gamma$ production at $\sqrt{s} = 1.8$ TeV in the electron and muon channels. The observed photon E_T spectra agree well with the Standard Model predictions, yielding limits on anomalous $WW\gamma$ and $ZZ\gamma$ couplings. In addition there is a hint of a

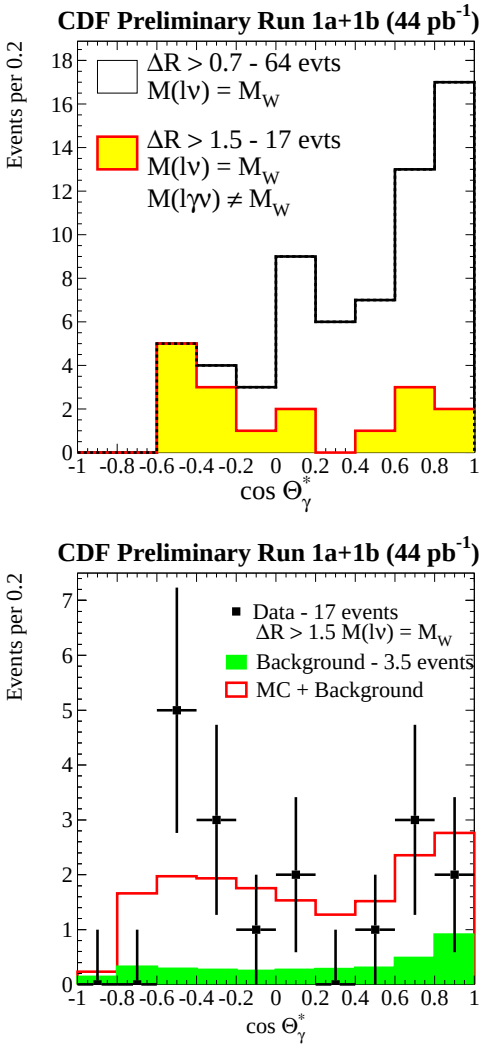

Figure 7: CDF distribution of (a) $\cos\theta^*$ for the loose cuts ($\Delta R > 0.7$) [open histogram] and the tight cuts ($\Delta R > 1.5$ and $M(\ell,\gamma,\nu) \neq M_W$) [shaded histogram] (b) $\cos\theta^*$, where the points are the data and the open histogram is the sum of the Standard Model prediction and the background estimate. The shaded histogram is the background estimate.

Table 9: CDF $W\gamma$ Gauge Zero
$W\gamma$ events CDF preliminary ($\sim 44\,\mathrm{pb}^{-1}$)
$M(\ell,\nu) = M_W$

	$0.7 < \Delta\mathrm{R} < 1.5$	$\Delta\mathrm{R} > 1.5$
$M(\ell,\nu,\gamma) = M_W$	25	13
$M(\ell,\nu,\gamma) \neq M_W$	9	17

gauge zero in $W\gamma$ events. CDF and DØ will continue to make significant contributions to Tri-Boson coupling measurements.

Acknowledgements

I am indebted to members of the CDF and DØ collaborations, whose assistance was invaluable in the preparation of this talk. It was a pleasure to present their fine work.

References

[1] K. Hagiwara *et al.*, Nucl. Phys. B **282**, 253 (1987).

[2] U. Baur and D. Zeppenfeld, Nucl. Phys. B **308**, 127 (1988).

[3] U. Baur and E.L. Berger, Phys. Rev. D **47**, 4889 (1993).

[4] U. Baur and E.L. Berger, Phys. Rev. D **41**, 1476 (1990).

[5] K.O. Mikaelian, Phys. Rev. D **17**, 750 (1978); K.O. Mikaelian, M.A. Samuel and D. Sahdev, Phys. Rev. Lett. **43**, 746 (1979 R.W. Brown, K.O. Mikaelian and D. Sahdev, Phys. Rev. D **20**, 1164 (1979); T.R. Grose and K.O. Mikaelian, Phys. Rev. D **23**, 123 (1981); C.J. Goebel, F. Halzen and J.P. Leveille, Phys. Rev. D **23**, 2682 (1981); S.J. Brodsky and R.W. Brown, Phys. Rev. Lett. **49**, 966 (1982); M.A. Samuel, Phys. Rev. D **27**, 2724 (1983); R.W. Brown, K.L. Kowalski and S.J. Brodsky, Phys. Rev. D **28**, 624 (1983); R.W. Brown and K.L. Kowalski, Phys.

Rev. D **29**, 2100 (1984); J. Cortés, K. Hagiwara and F. Herzog, Nucl. Phys. B **278**, 26 (1986).

[6] S. Abachi *et al.* Fermilab-Pub-95/042-E - *Submitted to PRL*